Optimum Exclusion Regions for Interference Protection in Device-to-Device Wireless Networks

Geordie George, Ratheesh K. Mungara, and Angel Lozano
Department of Information and Communication Technologies
Universitat Pompeu Fabra (UPF)
08018 Barcelona, Spain
Email:{geordie.george, ratheesh.mungara, angel.lozano}@upf.edu

***Abstract*—This paper addresses the benefits of introducing exclusion regions around both transmitters and receivers in D2D wireless networks. Such exclusion regions offer protection from interference at the expense of a sparser spatial reuse of spectrum, bringing about a tradeoff whose resolution entails optimizing the size of the exclusion regions as function of relevant system parameters. Our figure of merit for this optimization is the spectral efficiency. We first characterize this quantity for a given size of the exclusion regions, and then proceed to its optimization, altogether establishing the major benefits of incorporating properly sized exclusion regions in the applicable scheduling algorithms.**

I. Introduction

The addition of device-to-device (D2D) communication onto cellular and other infrastructure-based networks promises sizable improvements in performance provided there is sufficient spatial locality in the wireless traffic [1]–[6]. In overlay mode, in particular, a swath of spectrum is reserved for D2D traffic, thereby segregating it from both uplink and downlink. On this dedicated spectrum, D2D communication can achieve very dense bandwidth reuse and thereby very high system spectral efficiency (bits/s/Hz per unit area). Without a careful scheduling of the transmissions, however, a share of the D2D links experience strong interference from nearby unintended transmissions [7] and, as the density increases, this interference may progressively clog the network.

One way to mitigate this problem is to ensure that all co-channel D2D links, i.e., those occupying the same signaling channel (meaning a time-frequency signaling resource), respect certain exclusion regions. This restriction could then be incorporated into the scheduling policies, where it would have to be balanced with the need to service every link on one of the channels.

While exclusion regions offer protection from interference, thereby improving the link spectral efficiencies (bits/s/Hz per link) of the co-channel links, they also result in a sparser spectrum reuse and hence a tradeoff arises that requires an optimization of the exclusion regions. This optimization, and the ensuing benefits, are the theme of this paper.

This work was supported in part by Intel's University Research Program "5G: Transforming the Wireless User Experience" and by the MINECO Project TEC2012-34642.

Exclusion regions have been studied in the context of wireless ad-hoc networks [8]–[13], cognitive networks [14], [15] and D2D networks [16]–[19]. The existing works on ad-hoc networks explore this possibility in terms of transmission capacity [8], [9], defined as the maximum permissible density of simultaneous transmissions that satisfies a target receiver SIR (signal-to-interference ratio) with a specified outage probability, or else in terms of interference statistics [10], [11]. In this paper, instead, we focus on the ergodic spectral efficiency, arguably the most operationally relevant quantity in contemporary systems [20]. The contributions of the work are as follows:

- The analytical framework in [7] is extended to incorporate exclusion regions.
- The spatially averaged link and system spectral efficiencies are characterized in integral form, and they are further tightly approximated in closed form.
- By means of the foregoing analytical characterizations, the average system spectral efficiency is optimized over the size of the exclusion regions.

II. Network Geometry

We consider a D2D network with multiple links, each consisting of a transmitter and its intended receiver. The focus is on a specific channel occupied by a subset of *co-channel* links selected from a pool of *available* links such that there are no co-channel interferers within circular exclusion regions around each receiver.

The locations of the available transmitters are modeled as a homogeneous PPP (Poisson point process) $\Phi \subset \mathbb{R}^2$ of density λ, implying that on average there are λ available links per unit area. Each available transmitter has its intended receiver at a fixed distance r_0, and at a random angle uniformly distributed in $[0, 2\pi)$. The exclusion regions around the receivers have a radius $\delta \cdot r_0$ where $\delta \geq 0$ is the ratio of the exclusion radius to the intended link length r_0.

The average number of co-channel links per unit area, denoted by $\tilde{\lambda}$, depends on the exclusion radius δr_0 and on the type of channelization scheme as explained in the next section. The establishment of exclusion regions results in dependent thinning of the initial PPP Φ. Consequently, the

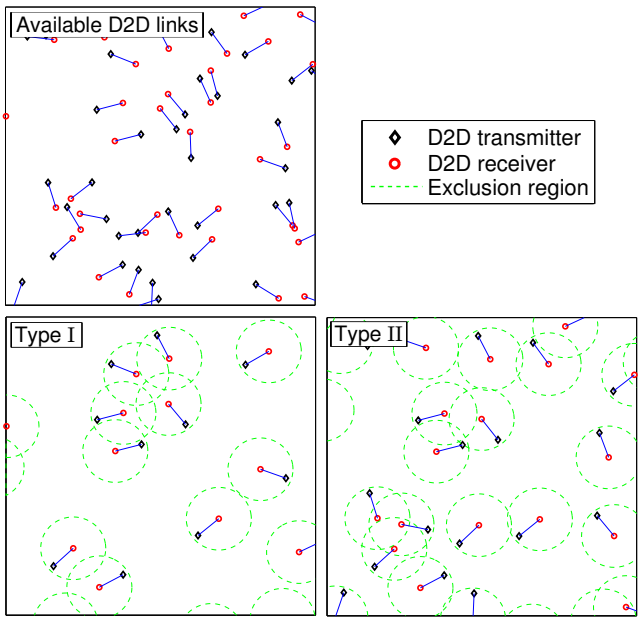

Fig. 1. Co-channel links under type I and type II channelization schemes performed on the same pool of available links.

locations of the co-channel transmitters no longer conform to a homogeneous PPP.

III. Channelization Schemes

To make the analysis as inclusive as possible, we consider two types of channelization schemes motivated by the Matérn hard core models type I and type II [21] commonly employed in the analysis of wireless ad-hoc networks [8], [9], [11], [18]. Though both types can achieve circular exclusion regions around the receivers as depicted in Fig. 1, for the same exclusion radius $\delta \mathsf{r}_0$ they result in a different $\tilde{\lambda}$.

A. Type I

In type I, an available link is allowed on the channel under consideration only when there is no interfering transmitter present inside the circle of radius $\delta \mathsf{r}_0$ centered at its receiver. The link is thus allowed with probability $p = e^{-\lambda \pi \delta^2 \mathsf{r}_0^2}$, which is the void probability of the PPP Φ (the probability that within a given area there exists no point of the PPP [22]) in the area $\pi \delta^2 \mathsf{r}_0^2$. Then, the average number of co-channel links per unit area becomes

$$\tilde{\lambda} = \lambda \, e^{-\lambda \pi \delta^2 \mathsf{r}_0^2}, \tag{1}$$

which is unimodal in λ. For a given δ, $\tilde{\lambda} \to 0$ as $\lambda \to \infty$. The maximum value of (1) is $\tilde{\lambda} = \frac{1}{e \pi \delta^2 \mathsf{r}_0^2}$, achieved at $\lambda = \frac{1}{\pi \delta^2 \mathsf{r}_0^2}$.

B. Type II

In type II, each available link is endowed with a random mark, uniformly distributed in $[0, 1]$, which may represent the time stamp or the priority of that link. An available link is allowed on the channel under consideration only when the following two conditions are met:

1) No transmitter with a lower mark is present inside a circle of radius $\delta \mathsf{r}_0$ around the link receiver.
2) No receiver with a lower mark is present inside a circle of radius $\delta \mathsf{r}_0$ around the link transmitter.

Inspired by existing works on scheduling/channelization for randomly distributed transceiver pairs [9], [11], [13], [18], we adopt the following approach to compute $\tilde{\lambda}$: consider a link with mark m. Since the marks are uniformly distributed in $[0, 1]$, the density of links with a mark lower than m is $m\lambda$ [22]. Condition 1 is based on the interfering transmitter locations relative to the given link, and Condition 2 is based on the interfered receiver locations, which also depend on the corresponding transmitter locations through the link distance r_0. Combining all that, we identify the transmitter locations that would violate Condition 2 and construct a resultant area, denoted by A_{II}, where no other transmitters must be present for both conditions to be satisfied.

Lemma 1. *The resultant area is*

$$A_{\text{II}} = \pi \, \xi(\delta) \, \mathsf{r}_0^2 \tag{2}$$

where

$$\xi(\delta) = \delta(\delta + 1) - \frac{2}{\pi^2} \int_{|\delta - 1|}^{\delta + 1} r \arcsin^2 \left(\frac{r^2 + 1 - \delta^2}{2r} \right) \mathrm{d}r \tag{3}$$

Proof. See Appendix A. ∎

The probability of allowing a link with random mark m is $p = e^{-m\lambda A_{\text{II}}}$ (which is the void probability of a PPP with density $m\lambda$ in the area A_{II} [22]). Then, the average number of co-channel links per unit area equals

$$\tilde{\lambda} = \lambda \int_0^1 e^{-m\lambda A_{\text{II}}} \mathrm{d}m \tag{4}$$

$$= \frac{1 - e^{-\lambda \pi \xi(\delta) \mathsf{r}_0^2}}{\pi \, \xi(\delta) \, \mathsf{r}_0^2} \tag{5}$$

where (5) follows from integration via (2). As per (5), $\tilde{\lambda}$ is monotonically increasing in λ and, as $\lambda \to \infty$,

$$\tilde{\lambda} \to \frac{1}{\pi \, \xi(\delta) \, \mathsf{r}_0^2} \tag{6}$$

(Recall that, in contrast, in type I we observed that $\tilde{\lambda} \to 0$ for $\lambda \to \infty$.).

Next, we develop an analytical model to characterize the spectral efficiency of a given link in a system with exclusion regions of radius $\delta \mathsf{r}_0$ and with the ensuing average number of co-channel links per unit area, $\tilde{\lambda}$.

IV. System Model

We place a receiver at the origin and locate its intended transmitter at a distance r_0. All interfering transmitters are located outside a circular exclusion region $\mathcal{B}(0, \delta \mathsf{r}_0)$, centered at the origin with radius $\delta \mathsf{r}_0$. The receiver at the origin observes

$$\mathsf{y} = \sqrt{\mathsf{P} \, \mathsf{r}_0^{-\eta}} \, \mathsf{H}_0 \, \mathsf{s}_0 + \mathsf{z} \tag{7}$$

where the first term is the signal from the intended transmitter while the second term is the interference

$$\mathsf{z} = \sum_{j=1}^{\infty} \sqrt{\mathsf{P}\,\mathsf{r}_j^{-\eta}}\,\mathsf{H}_j\,\mathsf{s}_j \tag{8}$$

made up from contributions from all other co-channel transmitters, with P the power measured at 1 m from its transmitter, $\eta > 2$ the pathloss exponent, r_j the distance between the jth transmitter and the receiver at the origin, H_j the corresponding fading, and s_j the symbol transmitted by the jth transmitter. The fading coefficients $\{\mathsf{H}_j\}$ are independent identically distributed (IID) complex Gaussian random variables with zero mean and unit variance, i.e., $\mathsf{H}_j \sim \mathcal{N}_{\mathbb{C}}(0,1)$ with each receiver privy only to the fading state of its own link. Likewise, $\mathsf{s}_j \sim \mathcal{N}_{\mathbb{C}}(0,1)$.

Since our objective is to assess the impact of interference and its mitigation, interference-limited conditions are presumed with thermal noise neglected.

Shadow fading, not considered here, could possibly be incorporated by adopting the approach in [23]. In a sense, shadow fading distorts the spatial geometry, which in our case would render the exclusion regions amorphous rather than circular.

V. Interference Model

A. Short-Term Distribution

Following the approach in [7], we model the short-term distribution of z as zero-mean complex Gaussian with matched conditional covariance $\sigma^2 = \mathbb{E}\left[|\mathsf{z}|^2 | \{\mathsf{r}_j\}\right]$, where the expectation is over the data and fading distributions. From (8), the conditional covariance σ^2, which represents the power of z for given interferer locations, is seen to equal

$$\sigma^2 = \sum_{j=1}^{\infty} \mathsf{P}\,\mathsf{r}_j^{-\eta}. \tag{9}$$

Besides the central limit theorem, there are information-theoretic arguments in favor of modeling the aggregate interference as complex Gaussian with a power dictated by the locations of the interferers: if the exact distribution of the interference is either unknown or ignored by the receiver, with a decoder designed to handle Gaussian noise, then the achievable spectral efficiency is precisely as if the interference were indeed Gaussian [24].

B. Spatial Distribution

As mentioned, the locations of the interfering transmitters do not conform to a PPP once exclusion regions are introduced. Even though the mean interference at the receiver could be computed exactly [10], [11], doing the same with the spectral efficiency appears unwieldy. Thus, we approximate the interferer locations with those of the points of a PPP $\tilde{\Phi}$ of density $\tilde{\lambda}$ present outside $\mathcal{B}(0, \delta \mathsf{r}_0)$, an approach that has been successfully applied to obtain the SIR distribution [8], [9] and whose goodness for our purposes is validated later in the paper.

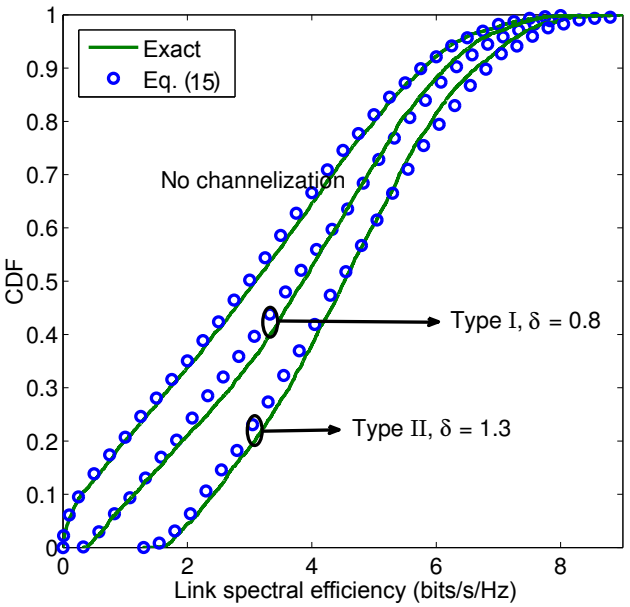

Fig. 2. CDF of link spectral efficiency for $\lambda = 40$ links/km^2, $\mathsf{r}_0 = 40$ m and pathloss exponent $\eta = 4.5$.

C. SIR

Applying our interference model, and recalling the intended signal term from (7), the instantaneous SIR of a given link is

$$\mathsf{SIR} = \frac{\mathsf{P}\,\mathsf{r}_0^{-\eta}\,\mathbb{E}\left[|\mathsf{H}_0\mathsf{s}_0|^2 \,|\, \mathsf{H}_0\right]}{\sigma^2} \tag{10}$$

$$= \varrho |\mathsf{H}_0|^2 \tag{11}$$

where the expectation is over s_0, conditioned on the known fading coefficient, with

$$\varrho = \frac{\mathsf{r}_0^{-\eta}}{\sum_{j=1}^{\infty} \mathsf{r}_j^{-\eta}} \tag{12}$$

the local-average SIR at the intended receiver.

Given the interferer distances $\{\mathsf{r}_j\}$, ϱ becomes determined and the instantaneous SIR in (10) is exponentially distributed with conditional CDF (cumulative distribution function)

$$F_{\mathsf{SIR}|\varrho}(\gamma) = 1 - e^{-\gamma/\varrho}. \tag{13}$$

VI. Link Spectral Efficiency

A. Specific Network Geometry

For a specific network geometry, i.e., for a given ϱ, the link spectral efficiency is

$$\mathsf{C}(\varrho) = \mathrm{E}\left[\log_2\left(1 + \varrho |\mathsf{H}_0|^2\right)\right] \tag{14}$$

$$= e^{1/\varrho} E_1\left(\frac{1}{\varrho}\right) \log_2 e \tag{15}$$

where $E_1(\zeta) = \int_1^{\infty} t^{-1} e^{-\zeta t} \mathrm{d}t$ is an exponential integral.

The following example validates the goodness of our interference model (Gaussian distribution and PPP approximation).

Example 1. Let $\lambda = 40$ links/km^2 with an intended link length of $\mathsf{r}_0 = 40$ m and with a pathloss exponent $\eta = 4.5$. Fig. 2

shows link spectral efficiency CDFs over many snapshots of $\{\mathsf{r}_j\}$. The *exact* curves give the mutual information (obtained through lengthy Monte-Carlo histograms and averaged over many fading realizations) with the locations of the interferers in (8) realized exactly under the respective channelization schemes and values of δ. Very good agreements are observed between these numerical values and Eq. (15) for type I with $\delta = 0.8$ and for type II with $\delta = 1.3$.

Similarly good agreements are observed for a variety of other settings, supporting our interference modeling approach.

B. Average Network Geometry

Next, we average the link spectral efficiency over all possible geometries.

Proposition 1. *For given λ and δ, the link spectral efficiency averaged over all network geometries is*

$$\bar{\mathsf{C}}(\lambda,\delta) = \log_2(e)\int_0^\infty \frac{1}{\gamma+1} \cdot e^{-\pi\tilde{\lambda}\delta^2\mathsf{r}_0^2\left[\frac{2}{\eta}E_{\frac{2+\eta}{\eta}}\left(\frac{\gamma}{\delta^\eta}\right)+\frac{\gamma^{2/\eta}}{\delta^2}\Gamma\left(1-\frac{2}{\eta}\right)-1\right]}\mathrm{d}\gamma \quad (16)$$

where $\tilde{\lambda}$ depends on λ and δ as per (1) for type I and (5) for type II, while $E_n(x) = \int_1^\infty \frac{e^{-xt}}{t^n}\mathrm{d}t$ is the generalized exponential integral and $\Gamma(\cdot)$ is the gamma function.

Proof. See Appendix B ∎

For $\delta = 0$, i.e., when there is no channelization and all available links are co-channel, taking $\lim_{\delta\to 0}\bar{\mathsf{C}}(\lambda,\delta)$ in (16) gives [7, Prop. 2]

$$\bar{\mathsf{C}}(\lambda,0) = \log_2(e)\int_0^\infty \frac{1}{\gamma+1}\, e^{-\gamma^{2/\eta}\,\pi\,\mathsf{r}_0^2\,\lambda\,\Gamma\left(1-\frac{2}{\eta}\right)}\mathrm{d}\gamma. \quad (17)$$

Simplified versions of Prop. 1 and (17) can be obtained by utilizing the approximation [25]

$$E_1(\zeta) \approx 4\sqrt{2\pi}\, a_N a_M \sum_{n=1}^{N+1}\sum_{i=1}^{M+1}\sqrt{b_n}e^{-4b_n b_i\zeta} \quad (18)$$

where N and M are positive integers that control the accuracy while the coefficients a_N, a_M, b_n and b_i are computed as described in [25, Sec. II]. Plugging this approximation into (15) and averaging over all geometries via ϱ, we obtain

$$\bar{\mathsf{C}}(\lambda,\delta) \approx 4\sqrt{2\pi}\, a_N a_M \log_2(e)\sum_{n=1}^{N+1}\sum_{i=1}^{M+1}\sqrt{b_n} \cdot \exp\left\{-\pi\tilde{\lambda}\,\delta^2\mathsf{r}_0^2\left[\frac{2}{\eta}E_{\frac{2+\eta}{\eta}}\left(\frac{[4b_nb_i-1]}{\delta^\eta}\right) + \frac{(4b_nb_i-1)^{2/\eta}}{\delta^2}\,\Gamma\left(1-\frac{2}{\eta}\right)-1\right]\right\} \quad (19)$$

where we again recall that $\tilde{\lambda}$ is a function of λ and δ, as given in (1) for type I and in (5) for type II. Similarly, for $\delta = 0$,

$$\bar{\mathsf{C}}(\lambda,0) \approx 4\sqrt{2\pi}\, a_N a_M \log_2(e) \cdot \sum_{n=1}^{N+1}\sum_{i=1}^{M+1}\sqrt{b_n}\, e^{-(4b_nb_i-1)^{2/\eta}\,\pi\,\mathsf{r}_0^2\,\lambda\,\Gamma\left(1-\frac{2}{\eta}\right)}. \quad (20)$$

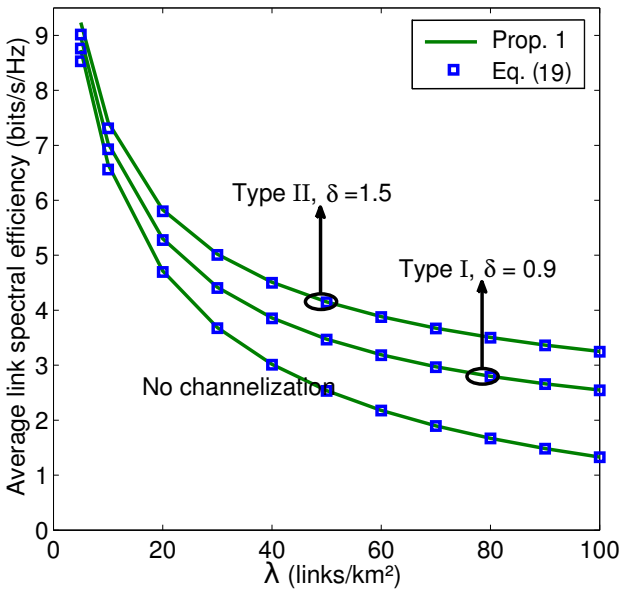

Fig. 3. Average link spectral efficiency as function of λ with $\mathsf{r}_0 = 40$ m and $\eta = 4.5$.

These closed forms, validated next, shall come handy in further analyses.

Example 2. Fig. 3 compares the spatially averaged link spectral efficiency in Prop. 1 with its approximation in (19), computed with $N = M = 50$. The average link spectral efficiencies are plotted for the case of no channelization ($\delta = 0$), for type I channelization with $\delta = 0.9$ and for type II channelization with $\delta = 1.5$.

VII. System Spectral Efficiency

The spatially averaged system spectral efficiency is obtained by scaling the spatially averaged link spectral efficiency by the average number of co-channel links per unit area, $\tilde{\lambda}$, giving

$$\bar{\mathcal{C}}(\lambda,\delta) = \tilde{\lambda}\log_2(e)\int_0^\infty \frac{1}{\gamma+1} \cdot e^{-\pi\tilde{\lambda}\delta^2\mathsf{r}_0^2\left[\frac{2}{\eta}E_{\frac{2+\eta}{\eta}}\left(\frac{\gamma}{\delta^\eta}\right)+\frac{\gamma^{2/\eta}}{\delta^2}\Gamma\left(1-\frac{2}{\eta}\right)-1\right]}\mathrm{d}\gamma \quad (21)$$

where, once more, $\tilde{\lambda}$ depends on λ and δ as per (1) for type I and (5) for type II.

VIII. Exclusion Region Size Optimization

To maximize the average system spectral efficiency for a given λ, the exclusion regions have to be optimally sized. This optimization returns

$$\bar{\mathcal{C}}^\star(\lambda) = \max_{\delta}\,\bar{\mathcal{C}}(\lambda,\delta) \quad (22)$$

and the argument that maximizes (22) is denoted by $\delta^\star(\lambda)$ while the value of $\tilde{\lambda}$ that ensues is $\tilde{\lambda}^\star(\lambda)$.

Example 3. Consider a D2D network with $\mathsf{r}_0 = 40$ m and pathloss exponent $\eta = 4.5$. Figure 4 plots $\bar{\mathcal{C}}^\star(\lambda)$ obtained numerically for both type I and type II channelizations.

The figure also shows the average system spectral efficiency without channelization, $\bar{\mathcal{C}}(\lambda, 0)$. The $\delta^\star(\lambda)$ and $\tilde{\lambda}^\star(\lambda)$ that indicate the correspondingly optimal exclusion size and average number of co-channel links per km^2 are respectively plotted in Figs. 5 and 6.

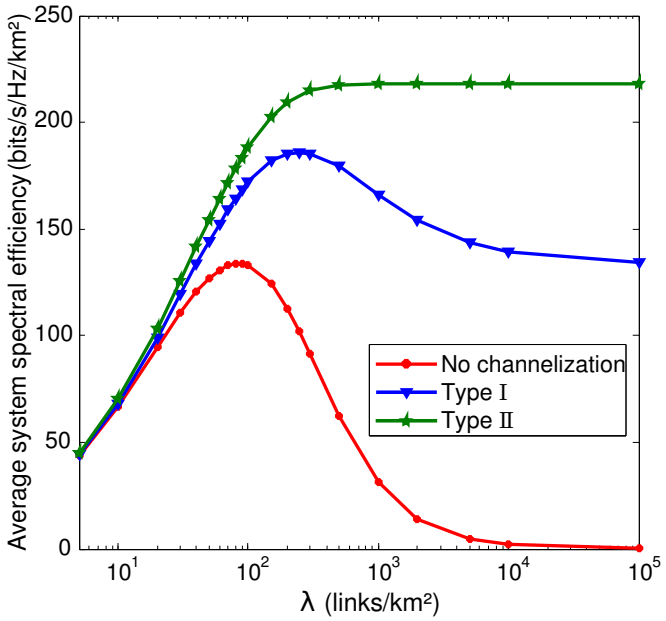

Fig. 4. Average system spectral efficiency (bits/s/Hz/km^2) as function of λ, for $r_0 = 40$ m and $\eta = 4.5$, with optimized δ.

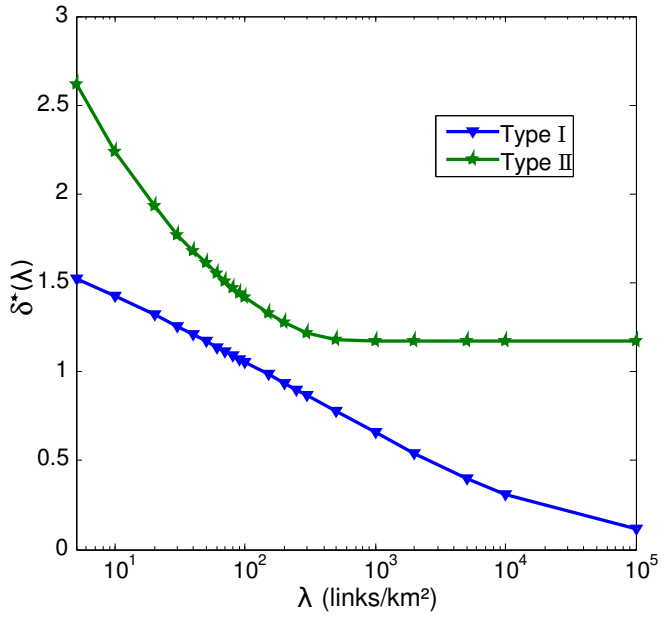

Fig. 5. Optimum δ as function of λ for $r_0 = 40$ m and $\eta = 4.5$.

Example 3 has been repeated for other values of r_0 and η to verify that the qualitative behavior does not change. This prompts the following observations:

- Both types of channelization dramatically outperform the no-channelization baseline in terms of the optimized system spectral efficiency, with type II markedly superior and monotonically improving in λ.
- The exclusion radius of type I diminishes with increasing λ, while type II maintains it at a value greater than the intended link distance, thereby protecting the links from close-by interferers.
- Though type I achieves higher $\tilde{\lambda}^\star(\lambda)$ than type II for many values of λ, it is inferior in terms of both link and system spectral efficiencies.

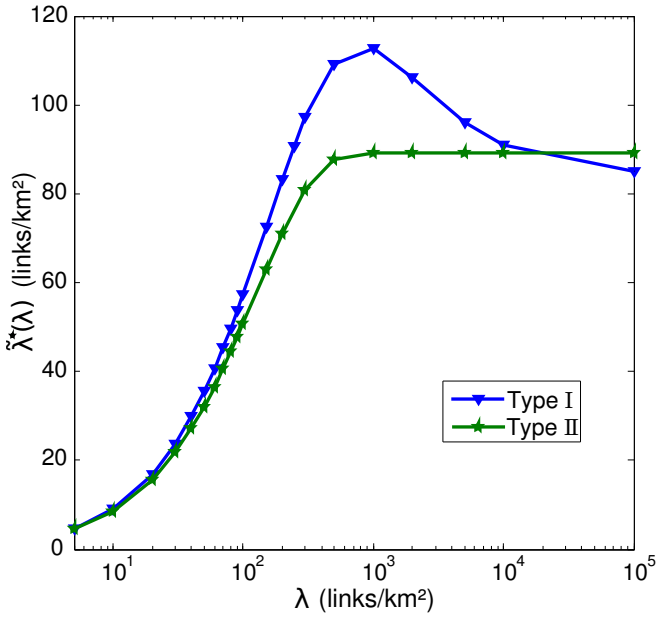

Fig. 6. Average number of co-channel links per km^2 as function of λ, for $r_0 = 40$ m and $\eta = 4.5$, with optimized δ.

Next, we characterize the peak values of the optimized system spectral efficiency under both types of channelization.

A. Type I

In this case, the peak value of the optimized system spectral efficiency is

$$\bar{\mathcal{C}}^{\star\star} = \max_{\lambda,\delta} \bar{\mathcal{C}}(\lambda, \delta) \tag{23}$$

and the arguments that maximize (23) are denoted by $\lambda^\star$ and $\delta_{\text{I}} = \delta^\star(\lambda^\star)$. In light of the transmission-capacity findings in [8], we conjecture that $\lambda^\star = \frac{1}{\pi \delta_{\text{I}}^2 r_0^2}$. We further conjecture that δ_{I} is independent of the intended link distance r_0.

To validate these conjectures, we observe that $\bar{\mathcal{C}}(\lambda, \delta)$ is unimodal in both λ and δ and, utilizing the approximation in (19), we differentiate $\bar{\mathcal{C}}(\lambda, \delta)$ w.r.t. λ and δ for arbitrary r_0. Armed with the resulting expression we analytically verify that, indeed, for specific values of η and the corresponding δ_{I} obtained numerically,

$$\frac{\partial \bar{\mathcal{C}}(\lambda, \delta)}{\partial \lambda}\Big|_{\delta=\delta_{\text{I}}, \lambda=\frac{1}{\pi \delta_{\text{I}}^2 r_0^2}} \approx 0 \tag{24}$$

$$\frac{\partial \bar{\mathcal{C}}(\lambda, \delta)}{\partial \delta}\Big|_{\delta=\delta_{\text{I}}, \lambda=\frac{1}{\pi \delta_{\text{I}}^2 r_0^2}} \approx 0 \tag{25}$$

TABLE I
TYPICAL VALUES OF δ_{I} AND $\kappa_{\text{I}}(\eta)$ FOR TYPE I

η	δ_{I}	$\kappa_{\text{I}}(\eta)$
3.8	0.8744	0.2282
4	0.8827	0.2482
4.5	0.8984	0.2976

TABLE II
TYPICAL VALUES OF δ_{II} AND $\kappa_{\text{II}}(\eta)$ FOR TYPE II

η	δ_{II}	$\kappa_{\text{II}}(\eta)$
3.8	1.1455	0.2625
4	1.1556	0.2873
4.5	1.1738	0.3486

where both zeroes are progressively approached as the accuracy of (19) is increased. For $\eta = 4.5$ and $N = M = 50$, e.g., the derivatives are within $\frac{10^{-16}}{\mathsf{r}_0^2}$ and $\frac{10^{-4}}{\mathsf{r}_0^2}$ of zero, respectively.

Substituting $\delta = \delta_{\text{I}}$ and $\lambda = \frac{1}{\pi \delta_{\text{I}}^2 \mathsf{r}_0^2}$ in (21), we can express the peak system spectral efficiency in the simple form

$$\bar{\mathcal{C}}^{\star\star} = \frac{\kappa_{\text{I}}(\eta)}{\mathsf{r}_0^2} \tag{26}$$

where

$$\kappa_{\text{I}}(\eta) = \frac{\log_2(e)}{e\,\pi\,\delta_{\text{I}}^2} \int_0^\infty \frac{1}{\gamma+1} \cdot e^{\frac{1}{e}\left[1-\frac{2}{\eta} E_{\frac{2+\eta}{\eta}}\left(\frac{\gamma}{\delta_{\text{I}}^\eta}\right) - \frac{\gamma^{2/\eta}}{\delta_{\text{I}}^2}\Gamma\left(1-\frac{2}{\eta}\right)\right]} \mathrm{d}\gamma \tag{27}$$

depends only on η. Values for δ_{I} and the corresponding $\kappa_{\text{I}}(\eta)$ for pathloss exponents spanning the entire range of interest for D2D are given in Table. I.

Plugging $\delta = \delta_{\text{I}}$ and $\lambda = \frac{1}{\pi \delta_{\text{I}}^2 \mathsf{r}_0^2}$ into (1), the average number of co-channel links per unit area corresponding to the peak is obtained as

$$\tilde{\lambda}^\star(\lambda^\star) = \frac{1}{e\pi\delta_{\text{I}}^2 \mathsf{r}_0^2}. \tag{28}$$

Thus, the average link spectral efficiency at the peak of the optimized system spectral efficiency equals

$$\frac{\bar{\mathcal{C}}^{\star\star}}{\tilde{\lambda}^\star(\lambda^\star)} = e\,\pi\,\delta_{\text{I}}^2\,\kappa_{\text{I}}(\eta) \tag{29}$$

which is independent of the link distance r_0 and a function of only the pathloss.

Another interesting observation is that the share of system area occupied by exclusion regions at the peak of the optimized system spectral efficiency equals, on average

$$\tilde{\lambda}^\star(\lambda^\star)\,\pi\,\delta_{\text{I}}^2\,\mathsf{r}_0^2 = 1/e. \tag{30}$$

B. Type II

In the case of type II, the optimized system spectral efficiency is bounded but monotonically increasing and thus its peak value is

$$\bar{\mathcal{C}}^{\star\star} = \max_{\delta} \lim_{\lambda\to\infty} \bar{\mathcal{C}}(\lambda, \delta) \tag{31}$$

where

$$\lim_{\lambda\to\infty} \bar{\mathcal{C}}(\lambda, \delta) = \frac{\log_2(e)}{\pi\,\xi(\delta)\,\mathsf{r}_0^2} \int_0^\infty \frac{1}{\gamma+1} \cdot e^{\frac{-\delta^2}{\xi(\delta)}\left[\frac{2}{\eta} E_{\frac{2+\eta}{\eta}}\left(\frac{\gamma}{\delta^\eta}\right) + \frac{\gamma^{2/\eta}}{\delta^2}\Gamma\left(1-\frac{2}{\eta}\right)-1\right]} \mathrm{d}\gamma \tag{32}$$

which follows from (16) and from the fact that $\tilde{\lambda} \to \frac{1}{\pi\xi(\delta)\mathsf{r}_0^2}$ as $\lambda \to \infty$. We again conjecture that the δ that solves (31) is independent of r_0, and denote it by $\delta_{\text{II}} = \delta^\star(\infty)$.

Since we observe that (32) is unimodal in δ, for specific values of η and arbitrary r_0 we verify analytically that the corresponding numerically obtained values of δ_{II} satisfy

$$\frac{\partial \bar{\mathcal{C}}(\infty, \delta)}{\partial \delta}\Big|_{\delta=\delta_{\text{II}}} \approx 0 \tag{33}$$

The differentiation is performed utilizing (19) with $\tilde{\lambda} = \frac{1}{\pi\,\xi(\delta)\,\mathsf{r}_0^2}$ and with the lower limit of the integral in (3) relaxed from $r = |\delta - 1|$ to $r = \delta - 1$ in light of the fact that $\delta_{\text{II}} > 1$ for the entire range of pathloss exponents relevant to D2D (cf. Table. II). The left side of (33) approaches zero as the accuracy of (19) is increased. For $\eta = 4.5$ and $N = M = 50$, e.g., zero is approached to within $\frac{10^{-5}}{\mathsf{r}_0^2}$.

Rewriting (32) with $\delta = \delta_{\text{II}}$, we can express $\bar{\mathcal{C}}^{\star\star}$ as

$$\bar{\mathcal{C}}^{\star\star} = \frac{\kappa_{\text{II}}(\eta)}{\mathsf{r}_0^2} \tag{34}$$

where

$$\kappa_{\text{II}}(\eta) = \frac{\log_2(e)}{\pi\,\xi(\delta_{\text{II}})} \int_0^\infty \frac{1}{\gamma+1} \cdot e^{-\frac{\delta_{\text{II}}^2}{\xi(\delta_{\text{II}})}\left[\frac{2}{\eta} E_{\frac{2+\eta}{\eta}}\left(\frac{\gamma}{\delta_{\text{II}}^\eta}\right) + \frac{\gamma^{2/\eta}}{\delta_{\text{II}}^2}\Gamma\left(1-\frac{2}{\eta}\right)-1\right]} \mathrm{d}\gamma \tag{35}$$

which depends only on η. Values for δ_{II} and the corresponding $\kappa_{\text{II}}(\eta)$ for typical pathloss exponents are given in Table II.

Letting $\lambda \to \infty$ and substituting $\delta = \delta_{\text{II}}$ in (5), we obtain the average number of co-channel links per unit area at the peak system spectral efficiency, $\tilde{\lambda}^\star(\infty) = \frac{1}{\pi\,\xi(\delta_{\text{II}})\,\mathsf{r}_0^2}$. Then, the average link spectral efficiency corresponding to the peak system spectral efficiency can be expressed as

$$\frac{\bar{\mathcal{C}}^{\star\star}}{\tilde{\lambda}^\star(\infty)} = \pi\,\xi(\delta_{\text{II}})\,\kappa_{\text{II}}(\eta) \tag{36}$$

which, interestingly enough, is independent of the link length r_0. The share of system area occupied by the exclusion regions equals, on average,

$$\tilde{\lambda}^\star(\infty)\,\pi\,\delta_{\text{II}}^2\,\mathsf{r}_0^2 = \frac{\delta_{\text{II}}^2}{\xi(\delta_{\text{II}})} \tag{37}$$

which depends only on the pathloss exponent.

IX. SUMMARY

As evidenced by Fig. 4, without a careful channelization the performance of a D2D network progressively collapses—because of interference—once the link density exceeds a

certain value that depends on the length of the links. With properly sized exclusion regions, though, this phenomenon is avoided. Although both types of channelization exhibit a satisfactory behavior in that respect, type II is able to find a markedly better tradeoff between the density of co-channel links and their individual spectral efficiencies. Conveniently, with type II the system spectral efficiency is monotonic in λ and thus there is no need to curb the system load at some fine-tuned value.

Compact forms for the optimum size of the exclusion regions and for the resulting system spectral efficiencies have been obtained as function of the key network parameters, facilitating intuition as to the effect of altering quantities such as the pathloss exponent or the length of the links.

Appendix A
Proof of Lemma 1

Consider the D2D link represented by the segment AB in Fig. 7, where A and B indicate the transmitter and the receiver locations, respectively. Let us identify the possible locations of other transmitters (with mark lower than AB) that could violate the conditions in Sec. III-B. Condition 1 is violated by the presence of other transmitters within the shaded circular region of radius $\delta \mathsf{r}_0$ around B, denoted by $\mathcal{B}_{\mathrm{B}}$. As for Condition 2, which is violated by the presence of other receivers within a circle of radius $\delta \mathsf{r}_0$ centered at A, the corresponding transmitter locations (r_0 away from each receiver at a uniformly distributed random angle) cannot be farther than $\delta \mathsf{r}_0 + \mathsf{r}_0$ from A. Hence, the D2D link AB could fail to satisfy the conditions only by the presence of lower-mark transmitters within the circle of radius $\delta \mathsf{r}_0 + \mathsf{r}_0$ centered at A and denoted by $\mathcal{B}_{\mathrm{A}}$.

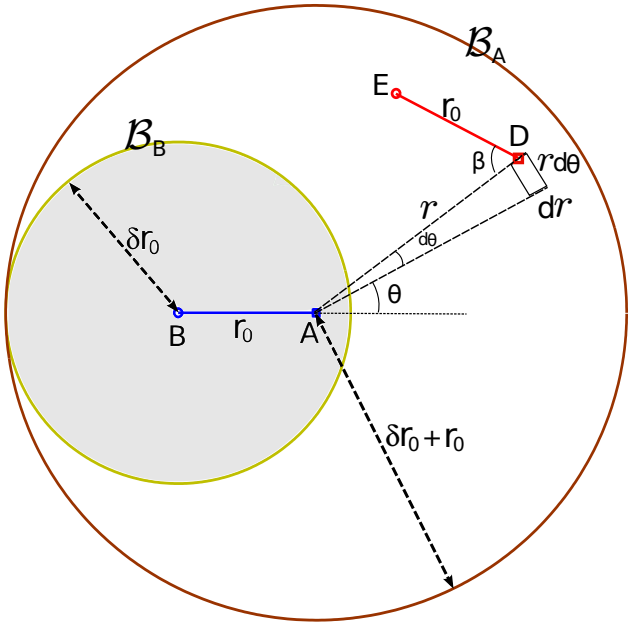

Fig. 7. Two neighboring D2D links under type II channelization scheme.

Since the presence of a lower-mark transmitter within $\mathcal{B}_{\mathrm{B}}$ will certainly violate the Condition 1, $\mathcal{B}_{\mathrm{B}}$ is part of A_{II}.

The presence of a lower-mark transmitter in the unshaded region within $\mathcal{B}_{\mathrm{A}}$ would violate Condition 2 only if the distance between its intended receiver and A is less than $\delta \mathsf{r}_0$. Consider a lower-mark transmitter denoted by D at a distance r and angle θ from A, as shown in Fig. 7. The presence of D can violate Condition 2 for AB with probability

$$p_1(r) = \frac{1}{\pi} \arccos\left(\frac{r^2 + \mathsf{r}_0^2(1-\delta^2)}{2r\mathsf{r}_0}\right) \tag{38}$$

which is the probability that the distance between its intended receiver E and A is less than $\delta \mathsf{r}_0$. This follows from the law of cosines and the fact that the angle β formed at D, between A and the D2D link DE, is uniformly distributed in $[0, \pi]$. Thus, the integration of $r\mathrm{d}\theta\,\mathrm{d}r$ scaled by $p_1(r)$ within the unshaded region is also part of A_{II}.

For the transmitter D to be within the unshaded region, the distance between B and D must be greater than $\delta \mathsf{r}_0$. Thus, when $\delta > 1$ as in the figure and D is within the unshaded region, r varies in $[\delta \mathsf{r}_0 - \mathsf{r}_0, \delta \mathsf{r}_0 + \mathsf{r}_0]$ while the angle θ, within the upper half of the unshaded region, varies in $[0, \theta']$ where

$$\theta' = \pi - \arccos\left(\frac{r^2 + \mathsf{r}_0^2(1-\delta^2)}{2r\mathsf{r}_0}\right).$$

Then, A_{II} can be computed as

$$A_{\mathrm{II}} = \pi\delta^2\mathsf{r}_0^2 + 2\int_{\delta\mathsf{r}_0-\mathsf{r}_0}^{\delta\mathsf{r}_0+\mathsf{r}_0}\int_0^{\theta'} p_1(r) r\,\mathrm{d}r\,\mathrm{d}\theta \tag{39}$$

$$= \pi\delta^2\mathsf{r}_0^2 + \int_{\delta\mathsf{r}_0-\mathsf{r}_0}^{\delta\mathsf{r}_0+\mathsf{r}_0} \frac{\pi r}{2} - \frac{2r}{\pi}\arcsin^2\left(\frac{r^2+\mathsf{r}_0^2(1-\delta^2)}{2r\mathsf{r}_0}\right)\mathrm{d}r \tag{40}$$

$$= \pi\mathsf{r}_0^2\delta(\delta+1) - \frac{2\mathsf{r}_0^2}{\pi}\int_{\delta-1}^{\delta+1} r\arcsin^2\left(\frac{r^2+1-\delta^2}{2r}\right)\mathrm{d}r \tag{41}$$

where the first term in (39) is the area of $\mathcal{B}_{\mathrm{B}}$ and the second term corresponds to the resultant area computed based on the transmitter locations within the unshaded region in $\mathcal{B}_{\mathrm{A}}$ that would violate Condition 2. Note that (41) is valid only for $\delta > 1$ as in Fig. 7. The result is generalized by replacing the lower limit of the integral with $|\delta - 1|$, which is the result in Lemma 1. This is because, when $0 < \delta < 1$, a transmitter present inside a circle of radius $\mathsf{r}_0 - \delta\mathsf{r}_0$ centered at A will always have its intended receiver located at a distance farther than $\delta \mathsf{r}_0$ from A and thereby cannot violate Condition 2.

APPENDIX B
PROOF OF PROPOSITION 1

The link spectral efficiency averaged over all possible geometries is computed as

$$\begin{aligned}
\bar{\mathsf{C}}(\lambda,\delta) &= \mathbb{E}[\mathsf{C}(\varrho)] && (42)\\
&= \mathbb{E}\left[\mathbb{E}\left[\log_2(1+\mathsf{SIR}|\varrho)\right]\right] && (43)\\
&= \mathbb{E}\left[\int_0^\infty \mathbb{P}[\log_2(1+\mathrm{SIR}|\rho) > t]\,\mathrm{d}t\right] && (44)\\
&= \mathbb{E}\left[\int_0^\infty \frac{\log_2 e}{\gamma+1}(1-F_{\mathsf{SIR}|\varrho}(\gamma))\,\mathrm{d}\gamma\right] && (45)\\
&= \int_0^\infty \frac{\log_2 e}{\gamma+1}\left(1-\mathbb{E}\left[F_{\mathsf{SIR}|\varrho}(\gamma)\right]\right)\,\mathrm{d}\gamma && (46)\\
&= \int_0^\infty \frac{\log_2 e}{\gamma+1}\left(1-F_{\mathsf{SIR}}(\gamma)\right)\,\mathrm{d}\gamma && (47)
\end{aligned}$$

where the outer and inner expectations in (43) are over ϱ and over the fading, respectively and (45) follows from the variable change $t=\log_2(1+\gamma)$. We next compute $F_{\mathsf{SIR}}(\gamma)$.

Putting (12) into (13), the conditional CDF of instantaneous SIR becomes

$$\begin{aligned}
F_{\mathsf{SIR}|\varrho}(\gamma) &= 1-e^{-\gamma\,\mathsf{r}_0^{\eta}\sum_{j=1}^{\infty}\mathsf{r}_j^{-\eta}} && (48)\\
&= 1-\prod_{j=1}^{\infty} e^{-\gamma\,\mathsf{r}_0^{\eta}\,\mathsf{r}_j^{-\eta}}. && (49)
\end{aligned}$$

Averaging (49) over the random interferer distances $\{\mathsf{r}_j\}$,

$$\begin{aligned}
F_{\mathsf{SIR}}(\gamma) &= 1-\mathbb{E}_{\Phi}\left[\prod_{j=1}^{\infty} e^{-\gamma\,\mathsf{r}_0^{\eta}\,\mathsf{r}_j^{-\eta}}\right] && (50)\\
&= 1-e^{-2\pi\tilde{\lambda}\int_{\delta\mathsf{r}_0}^{\infty}\left(1-e^{-\gamma\,\mathsf{r}_0^{\eta}\,x^{-\eta}}\right)x\mathrm{d}x} && (51)\\
&= 1-\exp\left\{-\gamma^{\frac{2}{\eta}}\,\pi\,\mathsf{r}_0^2\tilde{\lambda}\frac{2}{\eta}\int_0^{\frac{\gamma}{\delta^{\eta}}}\frac{1-e^{-u}}{u^{1+2/\eta}}\mathrm{d}u\right\} && (52)
\end{aligned}$$

where (51) follows from the definition of the probability generating functional of the PPP [22] and (52) follows from the variable change $\gamma\,\mathsf{r}_0^{\eta}\,x^{-\eta}=u$. Employing integration by parts in (52),

$$F_{\mathsf{SIR}}(\gamma) = 1-e^{-\pi\tilde{\lambda}\delta^2\mathsf{r}_0^2\left[\frac{2}{\eta}E_{\frac{2+\eta}{\eta}}\left(\frac{\gamma}{\delta^{\eta}}\right)+\frac{\gamma^{2/\eta}}{\delta^2}\Gamma\left(1-\frac{2}{\eta}\right)-1\right]}. \quad (53)$$

Plugging, (53) into (47) we obtain the claim in the proposition.

REFERENCES

[1] F. Boccardi, R. W. H. Jr., A. Lozano, T. Marzetta, and P. Popovski, "Five disruptive technology directions for 5G," *IEEE Commun. Mag.*, vol. 52, no. 2, pp. 74–80, Feb. 2014.

[2] J. G. Andrews, S. Buzzi, W. Choi, S. Hanly, A. Lozano, A. C. K. Soong, and J. C. Zhang, "What will 5G be?" *IEEE Journal on Sel. Areas in Communications*, vol. 32, no. 7, Jul. 2014.

[3] S. Andreev, A. Pyattaev, K. Johnsson, O. Galinina, and Y. Koucheryavy, "Cellular traffic offloading onto network-assisted device-to-device connections," *IEEE Commun. Mag.*, vol. 52, no. 4, pp. 20–31, Apr. 2014.

[4] L. Lei, Z. Zhong, C. Lin, and X. Shen, "Operator controlled device-to-device communications in LTE-advanced networks," *IEEE Wireless Commun. Mag.*, vol. 19, no. 3, pp. 96–104, Jun. 2012.

[5] G. Fodor, E. Dahlman, G. Mildh, S. Parkvall, N. Reider, G. Miklós, and Z. Turányi, "Design aspects of network assisted device-to-device communications," *IEEE Commun. Mag.*, vol. 50, no. 3, pp. 170–177, March 2012.

[6] X. Lin, J. Andrews, A. Ghosh, and R. Ratasuk, "An overview of 3GPP device-to-device proximity services," *IEEE Commun. Mag.*, vol. 52, no. 4, pp. 40–48, Apr. 2014.

[7] G. George, R. K. Mungara, and A. Lozano, "Overlaid device-to-device communication in cellular networks," in *Proc. IEEE Global Telecommun. Conf.*, Dec. 2014.

[8] A. Hasan and J. G. Andrews, "The guard zone in wireless ad hoc networks," *IEEE Trans. Wireless Commun.*, vol. 2, no. 3, pp. 897–906, Mar. 2007.

[9] F. Baccelli, J. Li, T. Richardson, S. Shakkottai, S. Subramanian, and X. Wu, "On optimizing CSMA for wide area ad-hoc networks," in *Proc. Int. Symp. on Modelling and Opt. in Mobile, Ad-hoc and Wireless Networks*, May 2011, pp. 354–359.

[10] M. Haenggi, "Mean interference in hard-core wireless networks," *IEEE Commun. Lett.*, vol. 15, no. 8, pp. 792–794, Aug. 2011.

[11] Y. Zhong, W. Zhang, and M. Haenggi, "Stochastic analysis of the mean interference for the RTS/CTS mechanism," in *Proc. IEEE Int. Conf. Commun.*, Jun. 2014, pp. 1996–2001.

[12] D. Torrieri and M. C. Valenti, "Exclusion and guard zones in DS-CDMA ad hoc networks," *IEEE Trans. Commun.*, vol. 61, no. 6, pp. 2468–2476, Jun. 2013.

[13] G. Alfano, M. Garetto, and E. Leonardi, "New directions into the stochastic geometry analysis of dense CSMA networks," *IEEE Trans. Mobile Comput.*, vol. 13, no. 2, pp. 324–336, Feb. 2014.

[14] S. Cho and W. Choi, "Relay cooperation with guard zone to combat interference from an underlaid network," in *Proc. IEEE Global Telecommun. Conf.*, Dec. 2011, pp. 1–5.

[15] C. H. Lee and M. Haenggi, "Interference and outage in Poisson cognitive networks," *IEEE Trans. Wireless Commun.*, vol. 11, no. 4, pp. 1392–1401, Apr. 2012.

[16] X. Wu, S. Tavildar, S. Shakkottai, T. Richardson, J. Li, R. Laroia, and A. Jovicic, "FlashLinQ: A synchronous distributed scheduler for peer-to-peer ad hoc networks," *IEEE/ACM Trans. Networking*, vol. 21, no. 4, pp. 1215–1228, Aug. 2013.

[17] N. Naderializadeh and A. S. Avestimehr, "ITLinQ: A new approach for spectrum sharing in device-to-device communication systems," *IEEE J. Select. Areas Commun.*, vol. 32, no. 6, pp. 1139–1151, Jun. 2014.

[18] R. K. Mungara, X. Zhang, A. Lozano, and R. W. H. Jr., "On the spatial spectral efficiency of ITLinQ," in *Proc. Annual Asilomar Conf. Signals, Syst., Comp.*, Nov. 2014.

[19] ——, "Performance evaluation of ITLinQ and FlashLinQ for overlaid device-to-device communication," in *Proc. IEEE ICC Workshop on Device-to-Device Communication for Cellular and Wireless Networks (ICC'15)*, Jun. 2015.

[20] A. Lozano and N. Jindal, "Are yesterday's information-theoretic fading models and performance metrics adequate for the analysis of today's wireless systems?" *IEEE Commun. Mag.*, vol. 50, no. 11, pp. 210–217, Nov. 2012.

[21] B. Matérn, "Spatial variation," *Lecture Notes in Statistics*, vol. 36, 1986.

[22] M. Haenggi, *Stochastic Geometry for Wireless Networks*. Cambridge, UK: Cambridge University Press, 2012.

[23] P. Madhusudhanan, J. G. Restrepo, Y. E. Liu, and T. X. Brown, "Carrier to Interference ratio analysis for the shotgun cellular system," in *Proc. IEEE Global Telecommun. Conf.*, Honolulu, USA, Nov. 2009, pp. 1–6.

[24] A. Lapidoth and S. Shamai, "Fading channels: how perfect need "perfect side information" be?" *IEEE Trans. on Inform. Theory*, vol. 48, no. 5, pp. 1118–1134, May 2002.

[25] A. A. Alkheir and M. Ibnkahla, "An accurate approximation of the exponential integral function using a sum of exponentials," *IEEE Commun. Lett.*, vol. 17, no. 7, pp. 1364–1367, Jul. 2013.